Thermally tunable polarization by nanoparticle plasmonic resonance in photonic crystal fibers

David Poudereux, , Manuel Caño-García José F. Algorri, Braulio García-Cámara, José M. Sánchez-Pena, Xabier Quintana, Morten A. Geday and José M. Otón

Abstract: A photonic crystal fiber selectively filled with silver nanoparticles dispersed in polydimethylsiloxane has been numerically studied via finite elements analysis. These nanoparticles possess a localized surface plasmon resonance in the visible region which depends on the refractive index of the surrounding medium. The refractive index of polydimethylsiloxane can be thermally tuned leading to the design of polarization tunable filters. Filters found with this setup show anisotropic attenuation of the x-polarization fundamental mode around $\alpha_x = 1200 dB/cm$ remarkably higher than the y-polarization mode. Moreover, high fiber birefringence and birefringence reversal is observed in the spectral region of the plasmon.

References and links

1. J. C. Knight, T. A. Birks, P. St. J. Russell, and D. M. Atkin, "All-silica single-mode optical fiber with photonic crystal cladding," Opt. Lett. **21**, 1547–1549 (1996).
2. R. Cregan, B. Mangan, J. Knight, T. Birks, P. S. J. Russell, P. Roberts, and D. Allan, "Single-mode photonic band gap guidance of light in air," Science **285**, 1537–1539 (1999).
3. R. Bise, R. Windeler, K. Kranz, C. Kerbage, B. Eggleton, and D. Trevor, "Tunable photonic band gap fiber," in *Optical Fiber Communication Conference and Exhibit* IEEE, OCF, 466–468 (2002).
4. T. Wolinski, K. Szaniawska, S. Ertman, P. Lesiak, A. Domanski, R. Dabrowski, E. Nowinowski-Kruszelnicki, and J. Wojcik, "Influence of temperature and electrical fields on propagation properties of photonic liquid-crystal fibres," Meas Sci Technol **17**, 985–991 (2006).
5. A. Piruska, I. Nikcevic, S. H. Lee, C. Ahn, W. R. Heineman, P. A. Limbach, and C. J. Seliskar, "The autofluorescence of plastic materials and chips measured under laser irradiation," Lab Chip **5**, 1348–1354 (2005).
6. F. Hua, Y. Sun, A. Gaur, M. A. Meitl, L. Bilhaut, L. Rotkina, J. Wang, P. Geil, M. Shim, J. A. Rogers *et al.*, "Polymer imprint lithography with molecular-scale resolution," Nano Lett. **4**, 2467–2471 (2004).
7. I. Pastoriza-Santos, J. Pérez-Juste, G. Kickelbick, and L. M. Liz-Marzán, "Optically active poly (dimethylsiloxane) elastomer films through doping with gold nanoparticles," J. Nanosci. Nanotechnol. **6**, 453–458 (2006).
8. C. Markos, K. Vlachos, and G. Kakarantzas, "Bending loss and thermo-optic effect of a hybrid pdms/silica photonic crystal fiber," Opt. Express **18**, 24344–24351 (2010).
9. H. Raether, *Surface Plasmons on Smooth Surfaces* (Springer, 1988).
10. S. A. Maier, *Plasmonics: Fundamentals and Applications* (Springer Science & Business Media, 2007).
11. E. Ozbay, "Plasmonics: merging photonics and electronics at nanoscale dimensions," Science **311**, 189–193 (2006).

12. P. N. Prasad, *Nanophotonics* (John Wiley & Sons, Inc., 2004).
13. K. A. Willets and R. P. Van Duyne, "Localized surface plasmon resonance spectroscopy and sensing," Annu. Rev. Phys. Chem. **58**, 267–297 (2007).
14. A. Ahmadivand and S. Golmohammadi, "Optimized plasmonic configurations: adjacent and merging regimes between a symmetric couple of Au rod/shell nano-arrangements for LSPR sensing and spectroscopic purposes," J. Nanopart. Res. **7**, 1–13 (2014).
15. J. Homola, "Surface plasmon resonance sensors for detection of chemical and biological species," Chem. Rev. **108**, 462–493 (2008).
16. R. Slavık, J. Homola, and J. Čtyroký, "Miniaturization of fiber optic surface plasmon resonance sensor," Sensor Actuat B-Chem **51**, 311–315 (1998).
17. M. Hautakorpi, M. Mattinen, and H. Ludvigsen, "Surface-plasmon-resonance sensor based on three-hole microstructured optical fiber," Opt. Express **16**, 8427–8432 (2008).
18. B. Shuai, L. Xia, Y. Zhang, and D. Liu, "A multi-core holey fiber based plasmonic sensor with large detection range and high linearity," Opt. Express **20**, 5974–5986 (2012).
19. X. Zhang, R. Wang, F. Cox, B. Kuhlmey, and M. Large, "Selective coating of holes in microstructured optical fiber and its application to in-fiber absorptive polarizers," Opt. Express **15**, 16270–16278 (2007).
20. A. Hassani and M. Skorobogatiy, "Design of the microstructured optical fiber-based surface plasmon resonance sensors with enhanced microfluidics," Opt. Express **14**, 11616–11621 (2006).
21. X. Yu, Y. Zhang, S. Pan, P. Shum, M. Yan, Y. Leviatan, and C. Li, "A selectively coated photonic crystal fiber based surface plasmon resonance sensor," J. Opt. **12**, 015005 (2010).
22. Y. Zhang, L. Xia, C. Zhou, X. Yu, H. Liu, D. Liu, and Y. Zhang, "Microstructured fiber based plasmonic index sensor with optimized accuracy and calibration relation in large dynamic range," Opt. Commun. **284**, 4161–4166 (2011).
23. N. Luan, R. Wang, W. Lv, Y. Lu, and J. Yao, "Surface plasmon resonance temperature sensor based on photonic crystal fibers randomly filled with silver nanowires," Sensors **14**, 16035–16045 (2014).
24. J. N. Dash and R. Jha, "Graphene-based birefringent photonic crystal fiber sensor using surface plasmon resonance," IEEE Photon. Technol. Lett., **26**, 1092–1095 (2014).
25. Q. Liu, S. Li, H. Chen, J. Li, and Z. Fan, "High-sensitivity plasmonic temperature sensor based on photonic crystal fiber coated with nanoscale gold film," Appl. Phys. Express **8**, 046701 (2015).
26. M. F. O. Hameed, A. Heikal, B. Younis, M. Abdelrazzak, and S. Obayya, "Ultra-high tunable liquid crystal-plasmonic photonic crystal fiber polarization filter," Opt. Express **23**, 7007–7020 (2015).
27. R. Caputo, and P. Giovanna, I. Melissa and L. De Sio, "Liquid Crystals as an Active Medium: Novel Possibilities in Plasmonics," Nanospectroscopy **1**,40–53 (2015).
28. L. Pezzi, L. De Sio, A. Veltri, T. Placido, G. Palermo, R. Comparelli, M.L. Curri,A. Agostiano, N. Tabiryan, and C.P. Umeton, "Photo-thermal effects in gold nanoparticles dispersed in thermotropic nematic liquid crystals," Phys. Chem. Chem. Phys. **17**, 20281–20287 (2015).
29. R. Caputo, L. De Sio, J, Dintinger, H. Sellame, T. Scharf, and C.P. Umeton, "Realization and characterization of POLICRYPS-like structures including metallic subentities," Mol. Cryst. Liq. Cryst. **553**, 111–117 (2012).
30. T. Maurer,J. Marae-Djouda,U. Cataldi,A. Gontier, G. Montay, Y. Madi,B. Panicaud,D. Macias, P.M. Adam, and G. Lévêque, T. B´urgi and R. Caputo "The beginnings of plasmomechanics: towards plasmonic strain sensors," Front. Mater. Sci. **9**, 170–177 (2015).
31. D. Poudereux, K. Mileńko, A. Dybko, J. M. Otón, and T. R. Woliński, "Polarization properties of polymer-based photonic crystal fibers," Photonics Lett Pol **6**, 59–61 (2014).
32. C. F. Bohren and D. R. Huffman, *Absorption and Scattering of Light by Small Particles* (John Wiley & Sons, 2008).
33. J. A. Scholl, A. L. Koh, and J. A. Dionne, "Quantum plasmon resonances of individual metallic nanoparticles," Nature **483**, 421–427 (2012).
34. J. Algorri, B. Garcia-Camara, A. Garcia-Garcia, V. Urruchi, and J. Sanchez-Pena, "Fiber Optic Temperature Sensor Based On Amplitude Modulation of Metallic and Semiconductor Nanoparticles in a Liquid Crystal Mixture," J. Lightwave Technol. **33**, 2451–2455 (2015).
35. X. Zheng, Y.G. Liu,Z. Wang, T. Han and B. Tai, "Tunable single-polarization single-mode photonic crystal fiber based on liquid infiltrating," IEEE Photon. Technol. Lett. **23**, 709–711 (2011).
36. P. Kumar,C. Paul, A. Datta, and N. Pani, "Highly birefringent photonic crystal fiber with negative dispersion and its propagation," in *2014 International Conference on Information Communication and Embedded Systems* (IEEE,2014), pp.1–6.
37. M. Kanehara, H. Koike, T. Yoshinaga, and T. Teranishi, "Indium tin oxide nanoparticles with compositionally tunable surface plasmon resonance frequencies in the near-ir region," J. Am. Chem. Soc. **131**, 17736–17737 (2009).
38. B. García-Cámara, R. Gómez-Medina, J. Sáenz, and B. Sepúlveda, "Sensing with magnetic dipolar resonances in semiconductor nanospheres," Opt. Express **21**, 23007–23020 (2013).
39. T. R. Jensen, M. D. Malinsky, C. L. Haynes, and R. P. Van Duyne, "Nanosphere lithography: tunable localized surface plasmon resonance spectra of silver nanoparticles," J. Phys. Chem. B **104**, 10549–10556 (2000).

1. Introduction

Photonic crystal fibers (PCFs) are optical fibers whose profile features a periodic or quasi-periodic structure parallel to the fiber axis. Typically the structures are holes in a silica matrix. The center core of the fiber may be solid or hollow. The hole diameters, the structure geometry, the periodicity and the materials can be tuned up in order to enhance specific properties of the fiber. This high versatility has made PCFs the target of many studies since their appearance in 1996 [1]. PCFs have been designed specifically to explore different properties like endlessly single-mode guiding, high birefringence, unusual chromatic dispersion or high nonlinearities [2].

Light in fibers is usually guided by modified Total Internal Reflection (mTIR). However, a second guiding mechanism, Photonic Band-Gap (PBG) guiding, appears in hollow core PCFs or in fibers whose core refractive index is lower than the cladding index. If the holes of a PCF with solid core are filled with a material having higher refractive index than the refractive index of the fiber material, the guiding mechanism of the light may evolve from mTIR to PBG [3,4].

Polydimethylsiloxane (PDMS) is especially suited for PCF infiltration. PDMS is a well characterized inexpensive silicon-based organic polymer. It has low autofluorescence [5] and is transparent at optical frequencies. Moreover, PDMS is flexible and has been used to mold structures of few nanometers [6] due to appropriate mechanical properties, being therefore ideal for fiber infiltration. The possibility of obtaining homogeneous samples of colloid nanoparticles (NP) in PDMS has also been reported experimentally [7].

Concerning photonic crystal fibers, PDMS features a refractive index (around 1.41) lower than silica, the most common material employed in PCF manufacturing. Moreover, PDMS shows an unusually large and negative linear thermo-optic coefficient i.e., the refractive index is highly temperature dependent [8].

Recent technological achievements allowing the fabrication of nanoparticles having different sizes and shapes have boosted the study of the interaction between light and these nanosystems. One of the most interesting effects of this interaction is the excitation of surface plasmon resonances (SPRs). SPRs result from the interaction between the free electrons of a metal in a metal-dielectric interface, and the electromagnetic field of the impinging light: they show up when the frequency of the incident photons matches the natural oscillation frequency of electrons [9–11]. In metallic nanoparticles, plasmon resonances are localized surface plasmon resonances (LSPRs) in contrast with propagating surface plasmon resonances (SPRs) on nanowires and other extended interfaces [12].

SPRs are characterized by a high sensitivity to variations in the refractive index of the environment [13,14]. This has been applied to the implementation of a number of sensing elements based on planar metallic layers structures [15] or metallic coatings around fibers [16]. The excitation of SPRs in PCFs with coated metal surfaces has been studied numerically [17,18] and experimentally [19]. Numerical analysis of PCF-based SPR sensors for liquids have been reported [20–22]; these sensors require selective hole filling. Recently SPR in silver nanowires [23] and in silver-coated graphene-based structures [24] have been simulated and a temperature sensor based on PCF coated with a nanoscale gold film [25] has been developed. SPRs in the anisotropic PCF show high anisotropic absorption in the resonance peak, thus being good candidates to build tunable in-fiber polarizers. Recently a polarization filter has been designed and theoretically studied using a hollow-core PCF filled with liquid crystal (LC) as waveguide and one of the cladding holes filled with gold [26].

All studies mentioned above refer to propagating SPRs in wires or surfaces coated with metals, where at least one of the dimensions is much larger than the light wavelength. Localized surface plasmon resonances (LSPRs) arise in structures where all dimensions are significantly smaller than the wavelength, like the nanoparticles mentioned above. LSPRs show some spe-

cific features that make them interesting in a number of applications. Since LSPRs are localized, light impinging the nanoparticles excite collective electron oscillations that enhance the near-field amplitude while decaying rapidly with distance from the nanoparticle. Unlike other SPRs, LSPRs can be excited directly without any complex wavevector coupling [12]; on the other hand, they are highly sensitive to the environment like any SPR. Their tiny size allows their use in subwavelength applications, such as nanoscale sensors [13]. Several studies have reported recently where LSRP has been used as the basic mechanism for obtaining sensors combined with liquid crystals [27, 28], holographic structures of polymers with LC, and the named POLICRYPS [29]. A new field has arisen named plasmomechanics that exploits the strain properties of PDMS doped with AuNP [30].

In this work, localized SPRs in silver nanoparticles (AgNP) have been theoretically studied eventually aiming to the simplicity of the mixture fabrication [30] and the filling process [31].NPs are commercial as well as PDMS, thus no technological effort to produce complex structures is necessary.

It is reported for the first time to our knowledge a tunable high birefringence photonic crystal fiber based a standard PCF with holes filled with AgNP dispersed in a matrix of PDMS. The same device could also be used as tunable in-fiber polarizer or as notch filter.

2. Theoretical considerations

For a proper analysis of the optical response of the mixture AgNP/PDMS, the effective refractive has been studied. The effective refractive index is calculated by the effective medium theory.

The Maxwell-Garnet effective medium theory [32] allows for the estimation of the AgNP/PDMS effective refractive index through the equation

$$\varepsilon_{av} = \varepsilon_m \left[1 + \frac{3f(\varepsilon - \varepsilon_m)/(\varepsilon + 2\varepsilon_m)}{1 - f(\varepsilon - \varepsilon_m)/(\varepsilon + 2\varepsilon_m)} \right] \tag{1}$$

where ε_m and ε are the electric permittivity of PDMS and AgNPs respectively, and f is the volume fraction of NPs in the composite.

Quantum effects inhibit the exact calculation of bulk properties at nanometric scale. Nevertheless it is possible to estimate the frequency evolution of the electric permittivity of the nanoparticles applying the Drude equation [33] given by

$$\varepsilon(\omega) = \varepsilon_\infty - \frac{\omega_p^2}{\omega^2 - i\gamma\omega} \tag{2}$$

where ω is the angular frequency of the incident light, ω_p is the plasmonic frequency of Ag, ε_∞ is a correction constant that accounts for the background electron screening at high frequency, and γ represents the scattering frequency of the electron as it travels through the materials.

Inclusion of scattering contributions according to Maxwell-Garnett theory was considered. However, preliminary experimental measurements showed that the scattering contribution cannot be influentially considered within the proposed frame of parameters.

3. Numerical analysis

Based on the above a numerical analysis of the refractive index dependence with temperature of AgNP-dispersed PDMS has been calculated. Figure 1 shows the results of real (top) and imaginary (bottom) parts of the effective refractive index of various AgNP-dispersed PDMS

suspensions. Different particle sizes (5 nm, 40 nm and 80 nm) and working temperatures (-10°C and 80°C) have been considered. The concentration has been set to 0.05%v/v in all cases. For this concentration the distance between particles is large enough to avoid coupling between plasmons. Both, real and imaginary components of the refractive index present a resonant mode corresponding to the LSPRs excited in the AgNPs at that given incident wavelength. LSPRs are clearly observed by comparison with the refractive index of PDMS (black crosses). Note that a slight variation in the refractive index of the thermally tuned PDMS induces a large change of the LSPR wavelength. As expected in nanoparticles so much smaller than the wavelength, the resonant frequency is scarcely modified by the NP concentration or size; however the spectral width and height of the resonant effect are affected: the resonant effect becomes more intense and narrower as the particle size or the concentration increase [34].

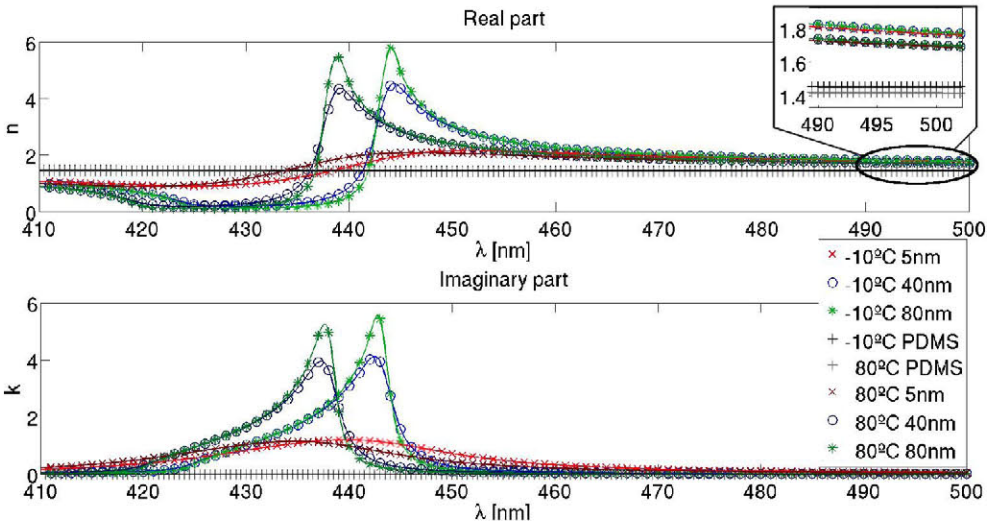

Fig. 1. Real and imaginary parts of the effective refractive index of PDMS with (and without) nanoparticles of 5 nm, 40 nm and 80 nm at -10°C and 80°C in the region of the AgNP LSPR.

As the temperature changes, the PDMS refractive index changes, producing a shift of the resonant mode of 5.2 nm in a range of 90°C. AgNPs behave as dopants, having strong influence on the refractive index just 30-40 nm about the resonance wavelength. Away from the plasmon wavelength the refractive indices approximate those of the pure PDMS. Mixing procedures of AgNP and PDMS have been described in the literature [30].

The AgNP-dispersed PDMS mixtures have been studied as infiltrations in a Photonic Crystal Fiber. A commercial PCF has been chosen. The fiber is polarization-maintaining (PM-PCF), what allows studying the attenuation anisotropy between two orthogonally polarized sets of guided modes. PM-PCF fibers are used to avoid coupling between modes and are highly important in both optical communication and fiber sensing systems. The specific fiber is PM-1550-01 (NKT Photonics), whose profile is shown in Fig. 2. The fiber has two large holes (4.5 μm diameter) symmetrically placed at both sides of the fiber axis, along with a number of concentrically distributed small cladding holes (2.2 μm diameter).

Collapsing the small holes (by fiber splicing, for example), the large holes can be easily infiltrated with liquids (or precured PDMS) [31]. Filling high viscosity liquids like PDMS occasionally requires applying positive pressure after collapsing the smaller holes to complete filling. In either case, PDMS is thermally cured afterwards.

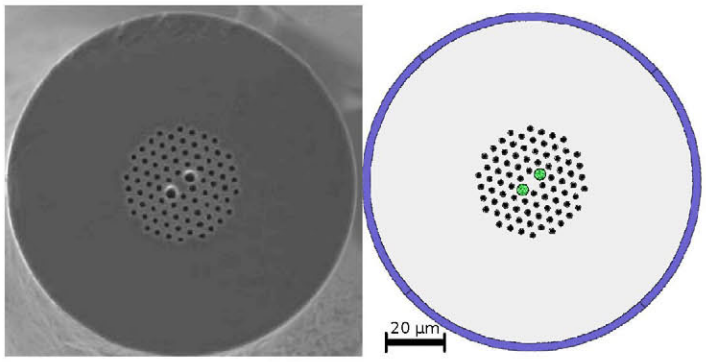

Fig. 2. Left: SEM image of PCF 1550-01, the asymmetry in the periodicity preserves the state of polarization. Right: geometric structure of the fiber, green holes are infiltrated with PDMS + AgNPs and external blue layer is the modeled PML boundary condition.

A model of the electric field distribution across the proposed structure has been prepared. The aim of the model is to determine the guided modes in spectral vicinity of the plasmon. Maxwell equations have been solved by finite element analysis. Note in Fig. 2 that the external layer of the PM-PCF has been modeled with Perfectly Matched Layer (PML) as absorbing boundary layer aiming to truncate the computational domain to keep the computational resource requirements reasonable. The simulations were carried out using commercially available COMSOL Multiphysics and were analyzed with MATLAB.

4. Results and discussion

As the refractive index of the material in the two bigger holes can be thermally tuned, the effective refractive index of the fundamental mode can be modulated as well. The temperature variation of each polarization is significantly different. Figure 3 shows the evolution of the normalized electric field profile of the fundamental mode of a PCF selectively filled in its bigger holes with AgNP/PDMS. The axis containing the two large holes (see Fig. 2) is taken as the x-axis, while the y-axis is orthogonal.

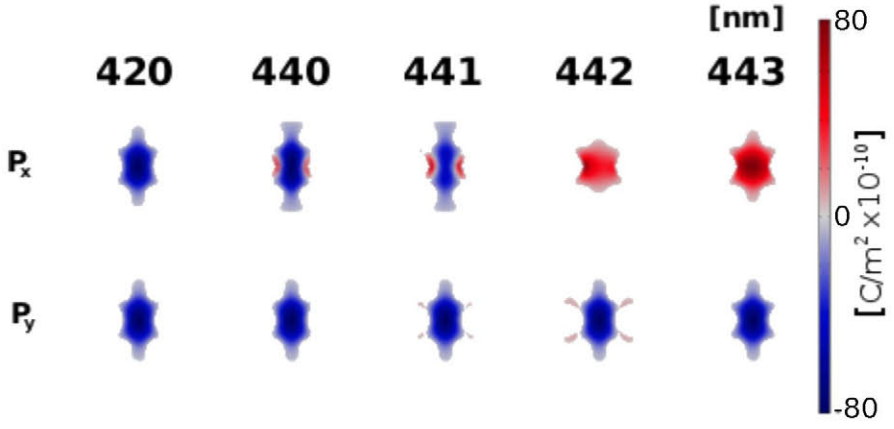

Fig. 3. x- and y-polarizations of the fundamental mode far (420 nm) and near the plasmon resonance (at 441.5 nm) of a PM-1550 selectively filled with PDMS doped with AgNP of 80 nm, 0.05 %v/v at 0°C.

Changes in the fundamental mode shape of x and y polarizations at 420 nm (far from the LSPR region) and just before and after the plasmon resonance (440∼442 nm) can be observed. The x-polarization is almost vanished near the resonance and its phase changes sharply once the resonance is passed. The y-polarization changes slightly near the resonance since the y-dimension of the large holes is not negligible.

Absorption in the SPR wavelength shows as a sharp peak of the imaginary part of the effective refractive index. Figure 4 shows the spectral variations of the refractive index components for x- and y-polarization fundamental modes. Light is guided in a PM-PCF selectively filled with PDMS doped with AgNP. Three different AgNP diameters have been used: 5, 40, and 80 nm. The absorption in the SPR wavelength can be seen as a sharp peak of the imaginary part of the effective refractive index. The refractive index of the environment dramatically affects the plasmonic response. Hence a change in the PDMS refractive index modifies the SPR wavelength.

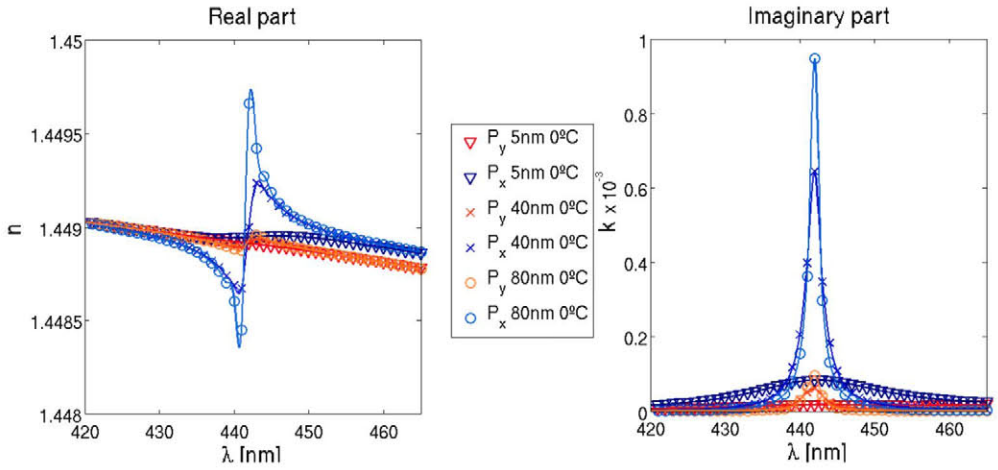

Fig. 4. Comparison of the effective refractive index, both real (left) and imaginary (right) parts, as a function of the Ag NP size and for both polarizations.

It should be noticed that the wavelength at which the resonance shows up is almost independent of the NP size. This is accordance with the theory because the wavelength of the impinging light is much longer than the NP size. However, the height of the real and imaginary peaks increase significantly for larger NP sizes. A comparative analysis of birefringence and attenuation of the fundamental mode for both polarizations has been carried out as well. It is well known that

$$B = \frac{\lambda}{2\pi}(\beta_y - \beta_x) = Re(n^y_{eff}) - Re(n^x_{eff}) \tag{3}$$

where B is the phase birefringence, β_x and β_y are the propagation constants of the two orthogonally polarized modes and $Re(n^y_{eff})$ and $Re(n^x_{eff})$ are the real part of the effective index of the y- and x- polarized modes, respectively.

The birefringence of three AgNPs of 5, 40 and 80 nm at 0°C is shown in Fig. 5. The birefringence of 80 nm AgNPs changes from 4.26×10^{-4} to -7.6×10^{-4} when passing the LSPR wavelength. These birefringences are fairly high [35, 36], and the birefringence shift, about $1.2\times10^{-3}$is noteworthy. Moreover this shift is thermally tunable. As the thermo-optic coefficient of the PDMS is very high, it is possible to thermally tune the wavelength where the plasmon resonance shows up. The imaginary part of the x-polarization, as seen in Fig. 6, is

remarkably higher than the y-polarization, and becomes sharper as the NP diameter increases. The LSPR shift is about 4.8 nm, which results in a sensitivity of 0.053 nm/ °C.

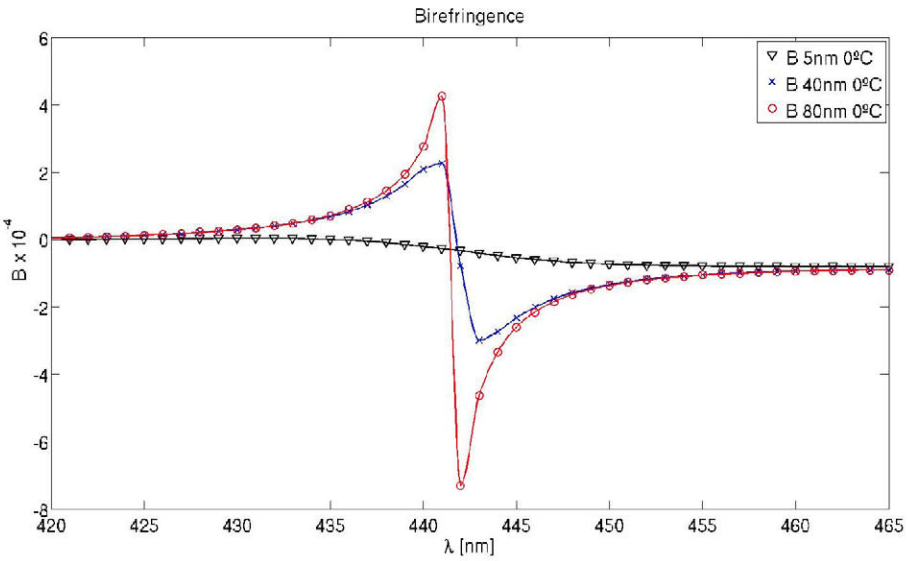

Fig. 5. Comparison of the birefringence of the system considering different sizes (particle diameter) of the AgNPs (5, 40 and 80 nm) at 0°C.

This sensitivity only depends on the thermo-optic coefficient of the PDMS and it is therefore independent of the NP size. This sensitivity is much higher than values obtained in sensors based on pure silica microcavities.

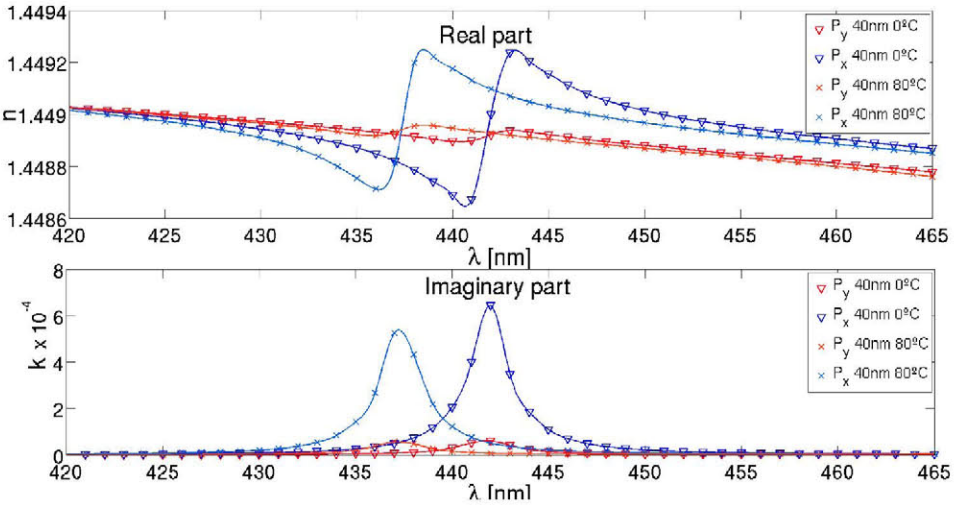

Fig. 6. Comparison of the effective refractive index, both real (upper panel) and imaginary (bottom panel) for both polarizations considering AgNPs of 40 nm (diameter) and temperatures of 0°C and 80°C.

To ascertain whether the device can work as a tunable in-fiber polarizer or as a notch filter, an analysis of the losses has been performed. Figure 7 shows that the attenuation for the x-

polarization fundamental mode of 80 nm AgNP at 0 °C is as high as $\alpha_x = 1200dB/cm$, while losses of the y-polarization are $\alpha_y = 118dB/cm$. Obviously the loss range of both polarizations can be controlled by making the infiltrated region of the required length. The ratio is similar in 40 nm NPs ($\alpha_{x40nm} = 795dB/cm$ and $\alpha_{y40nm} = 75dB/cm$) but lower in 5 nm NPs $\alpha_{x5nm} = 103dB/cm$ and $\alpha_{y5nm} = 23dB/cm$. These losses ranges demonstrate that a robust in-fiber tunable polarizer could be built in a less than 1 cm of fiber, even with a significant variation of the NP dimensions.

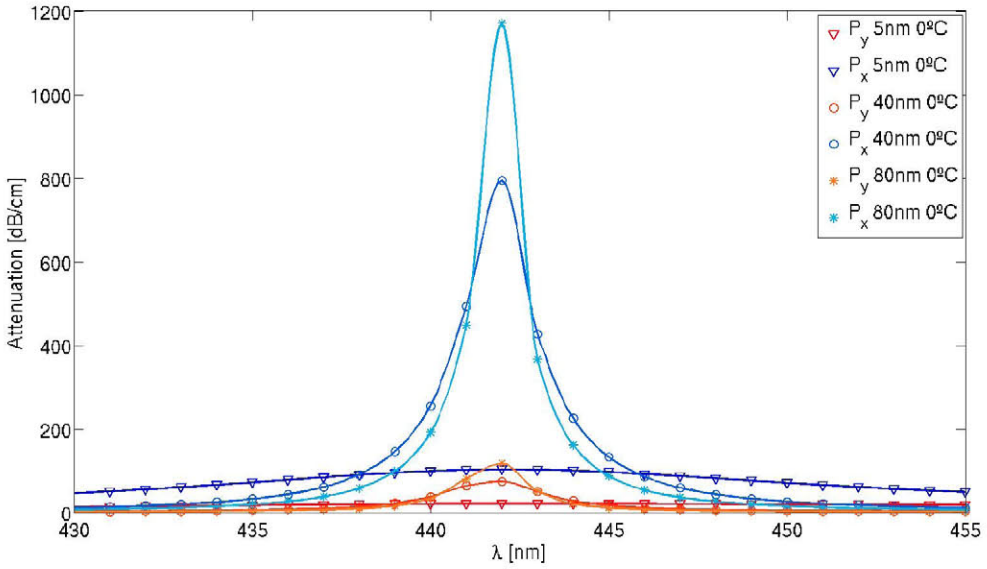

Fig. 7. Attenuation per cm of AgNP in 5, 40 and 80nm at 0°C of the x- and y-polarization of the fundamental mode.

It should be noticed that the light is always guided through the silica core of the PCF, whose associated attenuation is $< 0.15dB/m$ at 400 nm. Note also that, although the fiber is multimode in the visible region, the losses ratio of x/y-polarizations for higher-order guided modes remains similar to the fundamental mode ratio.

The spectral region where plasmon resonances show up largely depend on the material. Other kinds of NPs such as Indium Tin Oxide NPs [37] or Ag NPs with dielectric encapsulation of SiO_x [38, 39] show resonances in the infrared region. Consequently, the concepts shown in this work could be applied to filters or polarizers working in the optical communication windows.

5. Conclusion

An in-fiber tunable polarizer filter with a sensitivity about 0.053 nm/°C has been designed. The filter is based on a PM-PCF selectively filled with PDMS with dispersed silver nanoparticles. Numerical analysis demonstrates an attenuation of $\alpha_x = 1200dB/cm$ in the x-polarization fundamental mode and $\alpha_y = 119dB/cm$ for 80nm AgNPs. This asymmetry in the attenuation also occurs for higher guided modes, resulting in all guided modes with x-polarization being filtered out.

A change in the birefringence sign of the fiber is also observed. In the plasmon resonance region, the birefringence shift is remarkable, about 1.2×10^{-3}. The resonance can be thermally shifted about 5 nm.

All the parameters employed in the simulations have been set taking account an actual possibility of fabrication. The simple fabrication procedure, and the possibility to obtain the materials commercially make this kind of filters good candidates for actual device development.

Acknowledgments

Authors are grateful for financial support from Programa RETOS of the Spanish Ministerio de Economía y Competitividad (TEC2013-47342-C2), the regional R&D Program SINFOTON of the Comunidad de Madrid (SINFOTON S2013/MIT-2790) and European COST Action (IC1208).